Nanoscale

Cite this: *Nanoscale*, 2012, **4**, 6196

www.rsc.org/nanoscale

FEATURE ARTICLE

Nanoscale phase boundaries: a new twist to novel functionalities

J. X. Zhang,*[ab] R. J. Zeches,[c] Q. He,[d] Y.-H. Chu[ce] and R. Ramesh[ac]

Received 12th May 2012, Accepted 1st August 2012
DOI: 10.1039/c2nr31174g

In functional materials, nanoscale phase boundaries exhibit exotic phenomena that are notably absent in their parent phases. Over the past two decades, much of the research into complex oxides (such as cuprate superconductors, CMR manganites and relaxor ferroelectrics) has demonstrated the key role that nanoscale inhomogeneities play in controlling the electronic and/or ionic structure of these materials. One of the key characteristics in such systems is the strong susceptibility to external perturbations, such as magnetic, electric and mechanical fields. A direct consequence of the accommodation of a large number of cationic substitutions in complex oxides is the emergence of a number of physical phenomena from essentially the same crystal framework. Recently, multiferroic behavior, which is characterized by the co-existence and potential coupling of multiple ferroic order parameters, has captured considerable worldwide research interest. The perovskite, $BiFeO_3$, exhibits robust ferroelectricity coupled with antiferromagnetism at room temperature. A rather unique feature of this material system is its ability to "morph" its ground state when an external mechanical constraint is imposed on it. A particularly striking example is observed when a large (~4 to 5%) compressive strain is imposed on a thin film through the epitaxial constraint from the underlying substrate. Under these conditions, the ground state rhombohedral phase transforms into a tetragonal-like (or a derivative thereof) phase with a rather large unit cell (*c*/*a* ratio of ~1.26). When the epitaxial constraint is partially relaxed by increasing the film thickness, this tetragonal-like phase evolves into a "mixed-phase" state, consisting of a nanoscale admixture of the rhombohedral-like phase embedded in the tetragonal-like phase. Such a system gives us a new pathway to explore a variety of mechanical, magnetic and transport phenomena in constrained dimensions. This article reviews our progress to date in this direction and also captures some possible areas of future research. We use the electromechanical response and the magnetic properties as examples to illustrate that its novel functionalities are intrinsically due to the phase boundaries and not the constituent phases. The possible origin of the giant piezoelectric response and enhanced magnetic moment across the boundaries is proposed based on the flexoelectric and flexomagnetic effects.

1. Introduction

Phase boundaries in solids play a critical role in determining the macroscopic properties of materials.[1,2] In complex materials, such as strongly correlated oxides, phase boundaries can occur as a manifestation of the spatial variations of the spin, charge, orbital and lattice degrees of freedom. For example, in manganites and related systems, the phase separation and transition between an antiferromagnetic insulator and a ferromagnetic metal give rise to colossal magnetoresistance (CMR), where the response is maximized at the compositional boundary;[3–6] an analogous effect can be seen in high-temperature superconductors.[7–10] Other examples include the morphotropic-like phase boundaries in ferromagnets,[11,12] shape memory alloys[13] and relaxor ferroelectrics.[14–16] In the vicinity of the phase boundary (or the triple point in regions of three phase coexistence[17]), the free energies of two or three phases are nearly degenerate, resulting in a continuous variation in the local atomic/ionic/electronic structure from phase to phase.[18] The consequence of this behavior is that a small external perturbation can elicit a significant response, although the phase boundaries are randomly distributed in the material.[19]

The discovery of this exotic behavior from the phase boundaries described above[20–22] and the potential technological applications from these enhanced functionalities,[23,24] raises a fundamental question: how can these functional phase

[a]*Department of Physics, University of California, Berkeley, California, 94720, USA*
[b]*Department of Physics, Beijing Normal University, Beijing, 100875, China. E-mail: jxzhang@bnu.edu.cn*
[c]*Department of Materials Science and Engineering, University of California, Berkeley, California 94720, USA*
[d]*Advanced Light Source, Lawrence Berkeley National Laboratory, Berkeley, California, 94720, USA*
[e]*Department of Materials Science and Engineering, National Chiao Tung University, Hsinchu, 30010, Taiwan*

boundaries be assembled in an ordered way such that their properties can be controlled with a greater degree of freedom? Here, we take the epitaxially stabilized nanoscale phase boundaries in compressively strained multiferroic $BiFeO_3$ (BFO) as a model system to show the existence of a giant piezoelectric response and a remarkable enhancement of magnetism. Strain-induced flexoelectric or flexomagnetic effects are proposed to be the origin of these enhancements. We further propose that this behavior may not be unique to BFO and such engineered interphase interfaces can be a generic pathway to design new functionalities.

2. Phase coexistence in multiferroic BFO

Typically, functional phase boundaries in piezoelectrics or ferroelectrics arise as a consequence of inhomogeneous ionic or electronic charge distribution.[25–27] It has been demonstrated, however, that a morphotropic phase transition can be triggered by imposing hydrostatic pressures on ferroelectric $PbTiO_3$ (PTO) single crystals.[28,29] In addition, it has been observed that induced epitaxial strain can affect the morphotropic phase boundary in PZT thin films under ambient conditions. In our recent experimental and theoretical work, we demonstrated that epitaxial strain is a powerful pathway to accomplish the same goals of creating nanoscale mixed-phase ensembles in a lead-free material, such as $BiFeO_3$.

Epitaxial strain in oxide thin films and heterostructures is a powerful tool to induce emergent phenomena, which does not exist in their bulk counterparts. For example, researchers can now routinely modulate the structure of the epitaxial thin film by the lattice mismatch between the films and substrates;[30] for example, enhanced ferroelectricity has been reported in the $BaTiO_3/SrTiO_3/CaTiO_3$ artificial superlattice.[31] The effects of epitaxial strain have also been used to induce ferroelectricity from a non-ferroelectric ($SrTiO_3$[32]) or antiferroelectric material ($PbZrO_3$).[33] Apart from polarization, magnetization[34] and superconductivity,[35] recent experiments also show that the carrier concentration of a two dimensional electron gas at the $LaAlO_3$–$SrTiO_3$ interface can be strongly tailored by epitaxial strain.[36] With such a powerful control parameter, we started to search for potential candidates, which possess polymorphs, as a pathway to create a mixed-phase system. Among those oxides, BFO has gained great attention due to its room temperature multiferroicity.[37,38] In the ground state, BFO has a rhombohedral structure ($R3c$ symmetry) with a spontaneous polarization of $\sim$100 $\mu C\ cm^{-2}$ along its $\langle 111 \rangle$ pseudocubic diagonal. However, a number of theoretical studies have proposed that a new tetragonal phase ($P4mm$ symmetry) with a giant ferroelectric polarization of $\sim$150 $\mu C\ cm^{-2}$ can be stabilized.[39,40] Similar phases with large axial ratios have also been predicted in $BiCoO_3$ and $PbVO_3$.[41,42] As a result of these predictions, detailed work has begun to explore this new BFO phase in the context of its structure,[43–46] as well as its magnetic[47] and ferroelectric properties[48–54] and its optical response.[55,56]

According to recent density functional theory calculations,[57] when BFO is constrained by a compressive biaxial strain in excess of $\sim$5% along its a and b pseudocubic directions and simultaneously relaxed along its c pseudocubic direction, as shown in Fig. 1(a), the crystal will undergo a distinct structural transformation to a tetragonal-like phase. The degree of constraint is governed by the lattice mismatch between the BFO film and the underlying substrate as illustrated in Fig. 1(b), where it is shown that $LaAlO_3$ (LAO) substrates may provide an ideal template for bridging this abrupt change in the c/a ratio. Furthermore, *ab initio* calculations show that the total energy curve is almost flat with a c/a ratio between 1.1 and 1.3.[57] This suggests that a structural phase coexistence is energetically favorable at an intermediate strain state with a global energy minimum at $c/a = 1.25$ and a local energy minimum at $c/a = 1.1$. This phase coexistence has also been investigated from a

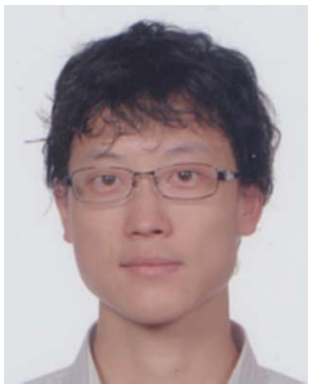

J. X. Zhang

Dr. Jinxing Zhang received his Ph.D in department of applied physics in the Hong Kong Polytechnic University in early 2010. Afterward, he held a postdoctoral position in department of physics in University of California, Berkeley, under the supervision of Professor R. Ramesh. In 2012, he has joined in department of physics, Beijing Normal University as a research professor. In recent years, he focuses on probing the emerging quantum phenomena in complex oxide thin film and nanostructures. He is also interested in the discovery of novel physical properties in functional materials with reduced dimensions.

R. J. Zeches

Robert Zeches graduated from the University of California, Berkeley with a Ph.D. in Materials Science and Engineering. His general research interests involve structure–property relationships in dimensionally constrained materials at the nanoscale. At Berkeley his research focused on using strain engineering to control the phase evolution of complex oxide thin films and the resultant enhancements in their piezoelectric, ferroelectric and magnetic properties. Prior to his work at Berkeley, he researched quantum confinement effects in semiconductor nanowires at NASA Ames. He is currently Senior Vice President of Product Development at Counterpoint Innovation Partners, and intellectual property aggregator in medical devices and clean technology.

macroscopic thermodynamic stability point of view and can be understood as the result of a competition between elastic, electrostatic and phase boundary energies.[58] With these theoretical predictions, the experimental studies on the formation of the nanoscale phase boundary and its influence on physical phenomena are the central focus of the following segments.

3. Stabilization of T- and R-like phase boundaries

The abundance of commercially available single crystal perovskite substrates allows for a large selection of unique templates for the growth of high-quality functional oxide thin films, particularly for perovskites.[59] The pseudocubic lattice constant for BFO is 3.96 Å in its bulk form. In principle, $GdScO_3$ single crystals permit the growth of strain-free BFO films due to their near-perfect lattice match.[60] The epitaxial growth of BFO films on $NdScO_3$ or $SmScO_3$ substrates can induce an in-plane tensile strain,[61] while growth on $SrTiO_3$ (STO), LAO or $YAlO_3$ (YAO) results in varying degrees of in-plane compressive strain (all the substrates adopt a pseudocubic or pseudotetragonal lattice).[62] It has been demonstrated that the ferroelectric polarization in BFO has a negligibly small dependence on the epitaxial strain up to 1.5%.[63] It has also been suggested that compressive or tensile strains up to 2.5% have a weak effect on the antiferromagnetic and ferroelectric order parameters in BFO.[64] An abrupt structural transition occurs when BFO is grown on YAO under an epitaxial strain of 6.7%.[57] The out-of-plane and in-plane lattice constants are ~4.71 Å and ~3.72 Å, respectively, with a slightly monoclinic angle of ~89°. This phase exhibits a depressed canted magnetic moment of ~2 emu per cc with a C-type antiferromagnetism,[65] which is different from the value of the rhombohedral ground state (4–6 emu per cc) with G-type antiferromagnetism.[66]

A similar tetragonal-like crystal structure with a slightly monoclinic distortion (subsequently referred to as the T-phase or

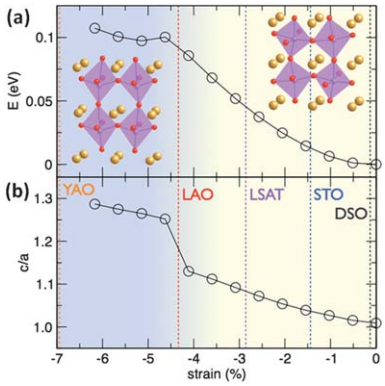

Fig. 1 (a) In-plane strain-dependent free energy of the BFO structure and (b) evolution of the *c*/*a* lattice parameter ratio as a function of the in-plane strain for BFO (the dashed lines indicate the mismatch strain from the different oxide substrates.

Q. He

Qing (Helen) He is an ALS Postdoctoral Fellow in Advanced Light Sources, Lawrence Berkeley National Laboratory. After receiving a B.S. degree from Tsinghua University, she did graduate work at the University of California, Berkeley, receiving an M.S. and Ph.D. in Physics. Her research interests involve employing soft X-ray based techniques to study different orders and their relationship in strongly correlated systems. She has received various awards, including the Jackson C. Koo Award from the University of California, Berkeley and the Ovshinsky Student Award from the American Physical Society.

Y.-H. Chu

Professor Ying-Hao Chu received his PhD in the Department of Materials Science & Engineering from National Tsing-Hua University in 2004. After that, he joined University of California, Berkeley as a postdoc. In 2008 he joined National Chiao Tung University in the Department of Materials Science & Engineering as an assistant professor. Currently, he is leading the atomic foundry of complex oxide as one part of Taiwan Consortium of Emergent Crystalline Materials. He is also affiliated with center for interdisciplinary science of National Chiao Tung University. His research is highly focused on complex functional oxides and nanostructures.

R. Ramesh

Professor R. Ramesh is currently the Plato Malozemoff Chair Professor in Materials Science and Physics at the University of California, Berkeley. He has initiated research in several key areas of oxide electronics, including ferroelectric nonvolatile memories, the colossal magnetoresistive effect at Bellcore and the University of Maryland. At Berkeley, he continues to pursue key scientific and technological problems in complex multifunctional oxide thin films, nanostructures and heterostructures. His current research interests include thermoelectric and photovoltaic energy conversion in complex oxide heterostructures.

T-BFO) is observed in BFO films (<20 nm thick) grown on LAO substrates (~4.5% lattice mismatch) when the in-plane compressive strain can be fully maintained. As the film thickness increases, however, a unique stripe-like feature emerges in the surface topography,[57] which is ascribed to the appearance of the rhombohedral-like (R) phase. The lattice constants of this distorted R-phase ((R-BFO); $a = b = 3.8$ Å, $c = 4.07$ Å) are different from the BFO bulk ground state. The fraction of stripe-like domains (R/T mixture) increases with the thickness due to further strain relaxation. For film thicknesses above 250 nm (ref. 67), the entire film is comprised of the R-phase. According to recent density functional calculations and X-ray diffraction studies, the structure of the R-BFO phase systematically evolves from the monoclinic *Cc* phase, resulting from the strain-induced deformation of the ground-state rhombohedral *R*3*c* phase; a further misfit strain of ~5% will deform BFO to the monoclinic *Cm* (T-BFO) phase.[68] Fig. 2(a) shows a representative atomic force microscopy (AFM) image of a 160 nm thick BFO film grown on an LAO substrate, where the stripe-like and flat areas indicate the mixed phase and T-BFO phase, respectively. X-Ray reciprocal space mapping (RSM) of this film gives preliminary information about its crystal structure.[68] As seen in Fig. 2(b), in addition to the peak for the T-like phase (labeled as T-BFO), a peak for the R-phase of BFO (subsequently referred to as the R-phase or R-BFO) can also be identified with an out-of-plane lattice constant of 4.07 Å. Four additional peaks (labeled as R′) suggest a complex phase coexistence in this partially relaxed T-phase film, which we define as mixed-phase BFO.

Transmission electron microscopy (TEM) provides direct atomic scale insight into the structure of such mixed phases. Fig. 3(a) shows a typical bright-field cross-sectional TEM image of a mixed-phase film. In this image, the inclined stripes ~20 to 30 nm in length can be seen to extend throughout the entire thickness of the film, corresponding to the stripe-like morphology observed in the topographical AFM image. The phase coexistence has also been confirmed *via* selective area electron diffraction (SAED) studies, shown in Fig. 3(b), where the two sets of diffraction spots are indexed as the T-phase and the R-phase. At high resolution (Fig. 3(c)) we observe a remarkably coherent interface between the two phases with a smooth transition of the out-of-plane lattice constant from 4.07 Å to 4.65 Å within 10–15 unit cells, with no observable dislocations, stacking faults or twinning across the phase boundary.

An iso-symmetric phase transition in this multiferroic perovskite, resulting from the combination of elastic/electric boundary conditions, has been proposed in several recent papers for

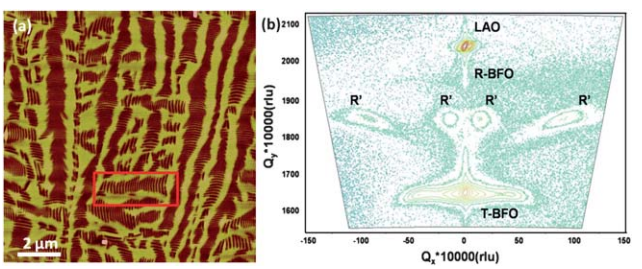

Fig. 2 (a) AFM image of a mixed-phase BFO film grown on an LAO substrate and (b) high-resolution X-ray RSM of a mixed-phase BFO film.

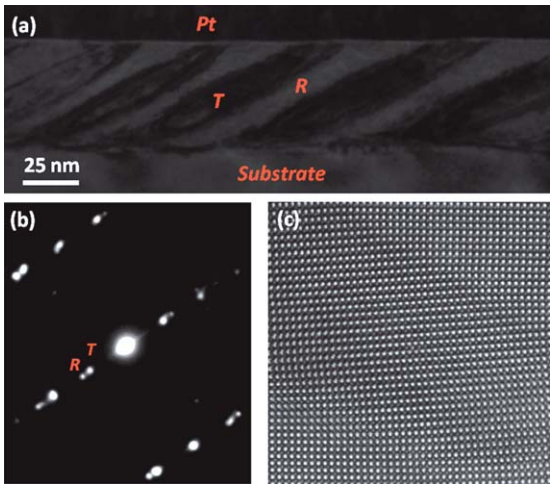

Fig. 3 (a) Low-magnification cross-sectional TEM image of a mixed-phase BFO film (the stripe-like feature is the phase coexistence of the R-like and T-like structures), (b) selected area electron diffraction pattern of a mixed-phase BFO film and (c) high-resolution TEM image across the T-like and R-like phase boundaries.

understanding the possible driving force behind the relaxation of this huge lattice mismatch (~14%) between the phases.[69–71] Such a phase transition is a first order phase transformation without a change of the space group symmetry;[72] however, it is accompanied by a change in the coordination and has been observed in crystals,[75] such as SmS, Ce, EuO and $(V_{0.963}Cr_{0.037})O_3$.[76–78] Here, both BFO phases, including the transition region, are believed to be monoclinic (*Cc* space group).[73,74] Ishibashi *et al.*[79,80] and Hatt *et al.*[71] described the details of the iso-symmetric transition in ferroelectrics using Landau–Devonshire theory and first-principles calculations. This was also followed by some recent theoretical papers related to the iso-symmetric oxygen octahedral rotation in other perovskites[81] and misfit shear-induced MPB between the R-/T-like interface,[82] suggesting its universal behavior in perovskites. Temperature and chemical substitution studies by XRD, AFM and micro-Raman techniques also provide detailed insight into these structural transitions.[81] We note that this iso-symmetric structure coexistence (with a big difference in the volume and *c*/*a* ratio) thus resembles a classical MPB. So, the next question is this: does this mixed phase ensemble undergo a phase transition under external stimuli, such as mechanical pressure, electric field or thermal activation? What is the associated electromechanical (or magnetoelectric) coupling response of the phase boundary?

4. Nanoscale phase transition and ultrahigh piezoelectric response

One good demonstration of the functionality of this nanoscale phase boundary is the giant electromechanical response. For piezoelectric materials, there is a wide range of applications from electromechanical actuators, transducers and sensors to micro-positioners.[83,84] Since the first demonstration of the piezoelectric effect by Pierre Curie and Jacques Curie in 1880, a large number of piezoelectric materials, including natural crystals (quartz, Rochelle salt *etc.*)[85] and artificially synthesized compounds

($BaTiO_3$ (BTO), $Pb(Zr_xTi_{1-x})O_3$ (PZT) *etc.*)[86,87] have been explored. PZT-based systems, with a d_{33} of ~500 pC N^{-1}, were the most widely used materials in the market until Park and Shrout reported an unprecedented d_{33} of ~2500 pC N^{-1} and strain of ~1.7% in solid solutions of $(1-x)Pb(Mg_{1/3}Nb_{2/3})O_3$–$xPbTiO_3$ (PMN–PT) or $(1-x)Pb(Zn_{1/3}Nb_{2/3})O_3$–$xPbTiO_3$ (PZN–PT). This breakthrough has been followed by a lot of work focused on understanding the fundamental mechanisms[26] and engineering the performance of these materials.[88]

The origin of the ultrahigh piezoelectricity in relaxor ferroelectrics is still a source of scientific debate, with a strong focus on the existence of an intermediate phase bridging the R- and T-like symmetries within the MPB.[89,90] However, it also seems to be favorable that nanoscale phase transitions[91] and randomly oriented nanoscale polar regions play critical roles in determining the enormous dielectric and piezoelectric responses.[19] A similar concept has been also imposed on BTO crystals, with an electric field induced strain of ~0.75%, using point defect-mediated reversible domain switching.[92] Compared to the MPB formed *via* chemical and valence mixing, a strain-driven phase coexistence in BFO provides a pathway to create well-ordered boundaries, which can then be used as a model system to investigate electromechanical and magnetoelectric coupling.

The electric field-dependent topography in mixed-phase BFO is illustrated in the AFM image in Fig. 4(a). In this figure, it can be seen that the application of an electric field can switch stripe-like regions into flat morphologies (indicated by the blue outer box) and a reversed electric field can switch the flat regions back to the mixed-phase (indicated by the red inner box). This reversible process is interpreted to be an electric field-induced structural phase transition, accompanied by a significant average surface displacement in this area of ~1 to 2 nm in ~100 nm thick films; *i.e.*, a field-induced strain of ~1 to 2%. On a more local scale, a surface displacement of ~5 to 6 nm is observed, as shown in Fig. 4(b)–(d). This ~5 to 6% electric field-induced strain is more consistent with the theoretically predicted maximum value of 6.6% for a full phase transition from the R-like ($c = 4.07$ Å) to T-like ($c = 4.65$ Å) phase with a ~45° inclination of the phase boundaries, as shown in Fig. 3(a).

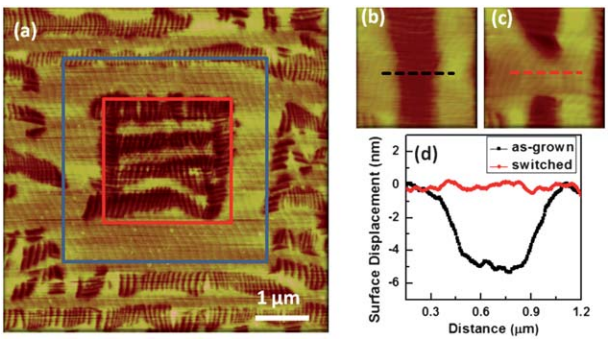

Fig. 4 (a) A large-area AFM image of a mixed-phase BFO film under electric field switching (the blue box indicates a +20 V probe bias switching and the red box indicates a −8 V probe bias switching), (b) a local AFM image of the mixed-phase before the application of an electric field, (c) the topography after the application of an electric field and (d) the line profile of the surface change indicated by the dashed lines in (b) and (c).

To confirm that the observations detailed above are the result of a field-induced structural phase transition and to gain more insight into its atomic-scale origins, *in situ* TEM experiments were conducted while electrically and mechanically perturbing the mixed-phase films.[93] Application of mechanical pressure using a nanoscale tip results in a structural change from the mixed-phase to the pure R-like phase accompanied by a 5% strain; while application of an electric field using a conductive nanoscale tip results in a structural change from the mixed-phase to the pure T-like phase with a negative 5% strain. The AFM and TEM evidence suggest that it is possible to achieve $a > 10\%$ cumulative strain *via* a combination of mechanical force and electric field by inter-converting the R- and T-like phases. This reversible strain is much higher than the one observed from relaxor ferroelectrics (~1.7%),[14] magnetostrictive materials (2%)[94] or the 90° domain wall motion in a clamping removed PZT film.[95] It is also comparable to the value from shape memory alloys.[96]

A common measure is the longitudinal piezoelectric coefficient, d_{33}, which is the induced strain in the material per unit of applied electric field in the same direction as the strain. To measure the average d_{33} response in mixed-phase BFO films, AC and DC electric fields are simultaneously applied *via* the AFM-based system. Measurements taken on large-area capacitors demonstrate a higher d_{33} of ~120 pm V^{-1} compared to measurements on pure R-like (65 pm V^{-1}) and pure T-like (30 pm V^{-1}) films. These results are consistent with the 1–2% strain under an electric field of 1000 kV cm^{-1} discussed previously in Fig. 4(a). Local measurements using just the AFM tip as a top-electrode in contact with a single R/T phase boundary result in a closed hysteresis loop during the sweeping of a DC bias, as shown in Fig. 5(a), along with that of the pure R-phase BFO calibration sample.[97] From these results, a maximum effective d_{33} of ~400 to 500 pm V^{-1} can be obtained. The peaks in the hysteresis curves can be attributed to the local phase transitions and the movement of the phase boundary underneath the probe tip, as illustrated by the schematics in Fig. 5(b) and (c). The process is reversible since the characteristic hysteresis curves can be repeatedly obtained by cycling the applied DC voltage. The measurements detailed above are quasi-static and, thus, it is expected that high-frequency measurements that are able to capture the signal at the moment of the phase transition might reveal a much higher d_{33} value in this small length scale.

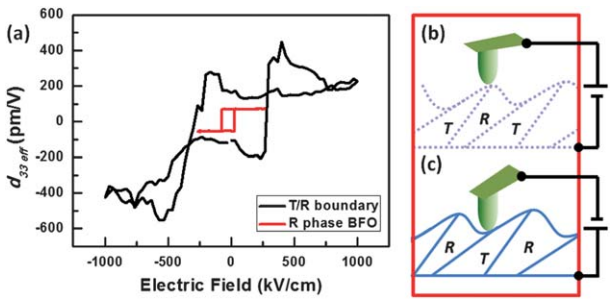

Fig. 5 (a) Effective piezoelectric constants from a single-phase boundary in a mixed-phase BFO film (blue) and from a pure R-phase BFO film (red); (b) and (c) show schematic diagrams of the conductive AFM tip and the R-like/T-like phase boundary under the (b) positive field and (c) negative field.

These results demonstrate that the ultra-high piezoresponse mainly arises from the displacement of the nanoscale morphotropic-like phase boundary. Although the limits of the piezoelectric response are still unclear, the well-ordered nanoscale phase boundaries provide us with an analogous model to maximize the electromechanical coupling in a lead-free system and better understand the physics in relaxor ferroelectrics.

5. Magnetic response

Electrical control of magnetism using magnetoelectrics and multiferroics at room temperature has attracted much attention recently.[98–104] The discovery of magnetoelectric coupling in BFO provides the potential to realize the electrical control of magnetic exchange coupling in engineered heterostructures.[38] Although the coexistence of ferromagnetic and ferroelectric order parameters in the same material seems to be theoretically unfavorable,[105] the coupling of electric and magnetic dipoles in a single-phase material at room temperature is still scientifically interesting and technologically valuable. There is a large body of theoretical and experimental work describing the magnetic structure of BFO,[106,107] which provides insight into the origin of the observed canted magnetic moment in the ground state R-phase of BFO.[108] The aforementioned discovery of a new crystal symmetry of BFO and the dramatic electric field-induced structural phase transition in this material encourages renewed experimental efforts to examine its magnetic ordering as well. For example, a very recent neutron scattering study in T-BFO revealed that two antiferromagnetic transitions happen at 324 K (G-type) and 260 K (C-type), respectively.[108]

X-Ray magnetic circular dichroism (XMCD) is a powerful experimental technique to study the spin and orbital magnetic moment in a material.[109] In the case of transition metals, such as iron, 2p electrons can be excited to the 3d state *via* incident circularly polarized X-rays with energies in excess of 700 eV, where the resulting spectrum includes magnetic information. We have employed this technique to study BFO by examining the magnetic response of T-phase, mixed-phase and fully relaxed R-phase films for comparison. The results of these studies can be seen in Fig. 6. In Fig. 6(a), the XMCD data shown for all three types of film represent the difference between the X-ray absorption spectra (XAS) obtained with an applied 2 T magnetic field in parallel and antiparallel directions with respect to the ***k***-vector of the incident X-rays with fixed polarization. The red curves in Fig. 6(a) represent data from pure R-phase BFO films, which exhibit a relatively negligible XMCD signal due to the canted moment being only ~6 to 8 emu per cc.[110] The green curves in Fig. 6(a) represent data from pure T-like phase films and show a negligible XMCD signal, which is consistent with the symmetry constraints that do not allow canting of the Fe^{3+} spins.[71] This magnetic signal has been further confirmed by conventional SQUID measurements. The black curves in Fig. 6(a) represent data from mixed-phase BFO films and show a significantly stronger XMCD signal, indicating a higher magnetic moment. In Fig. 6(b), the XMCD data represent the difference between the XAS obtained for left and right circularly polarized (LCP and RCP) incident X-rays with an applied 4 T magnetic field. It can be seen in this figure that the LCP and RCP X-rays have reversed the polarities with respect to each other, confirming that the response is magnetic in origin. Both of the complementary measurements shown in Fig. 6(a) and (b) clearly

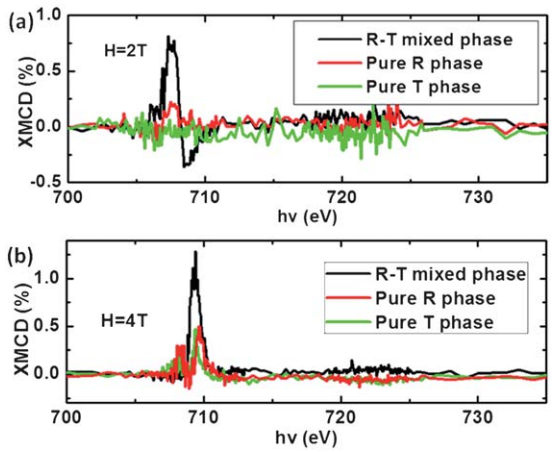

Fig. 6 (a) XMCD spectra of three different kinds of film probed by fixed X-ray circular polarization (right circularly polarized) under an applied 2 T magnetic field in parallel and antiparallel orientations with respect to the ***k***-vector of the incident X-rays and (b) XMCD spectra of three different kinds of film measured with X-ray polarization switched between right circular and left circular polarization under an applied constant magnetic field of 4 T.

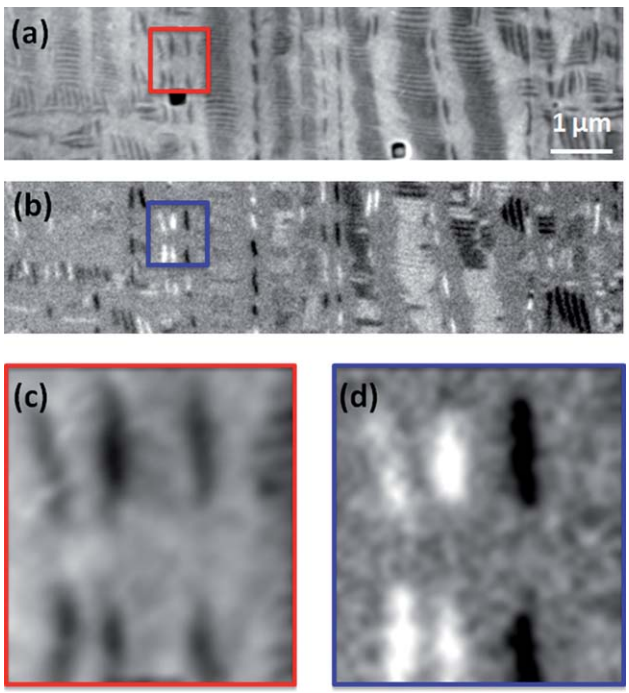

Fig. 7 (a) A PEEM image with left circularly polarized X-rays providing mainly structural contrast (darker stripes are the R-like phase and bright areas are the T-like phase), (b) a XMCD-PEEM image showing enhanced magnetic contrast derived from the ratio of the PEEM images taken with left and right circularly polarized X-rays at the same location (black and white contrast indicates magnetic moments pointing parallel and antiparallel relative to the incident X-rays), (c) a magnified topographical structure and (d) the detailed magnetic moment information around the phase boundaries associated with (c).

reveal the existence of a spontaneous magnetic moment in the mixed-phase samples. From the ~1% XMCD signal and using data for other oxide systems (manganites, Fe_3O_4)[111] as a semi-quantitative calibration, we estimate the magnetization in mixed-phase BFO to be on the order of 30–40 emu per cc.

To explore the microscopic origins of this enhanced magnetic moment, the XMCD signal was mapped out using photoemission electron microscopy (PEEM), which provides the spatial resolution to study the magnetic systems. Regions with a magnetic moment lying parallel to the X-ray wave vector show bright contrast, while those that are antiparallel show dark contrast. The PEEM images obtained *via* incident LCP X-rays at $\phi = 0°$ are shown in Fig. 7(a) and (c) and show mainly topographical contrast. The PEEM images shown in Fig. 7(b) and (d) reveal the intrinsic magnetic contrast in the mixed-phase films. Bright and dark stripe-like patterns, as seen in Fig. 7(d), indicate that these stripes have magnetic moments lying parallel and antiparallel to the incident X-rays. When the sample is rotated by 180°, all of the stripes reverse contrast, further confirming the magnetic origin. These experiments strongly suggest that the enhanced magnetic moment in mixed-phase films comes primarily from the nanoscale phase boundaries.

This spontaneous magnetization at antiferromagnetic phase boundaries provides a basis for renewed scientific interest in the search for coexisting ferroelectric and magnetic moments at room temperature. Furthermore, with these results combined with those demonstrating the deterministic control of the phase concentration *via* an applied electric field, there is renewed potential for the electrical manipulation of magnetism at room temperature.

6. Possible origins and future directions

The physical phenomena associated with nanoscale phase boundaries reviewed here have the potential to trigger a great deal of interest, ranging from fundamental scientific research to practical technological applications. If a strain profile is carefully mapped across the phase boundary with the bulk R-phase as the ground state, we expect to obtain a distinct strain gradient between R-like (pink shadow) and T-like phases (blue shadow) bridged by the ~5 nm phase boundary (green shadow) as shown in Fig. 8(a). The strain gradient induced here is much larger than the one observed in other ferroelectrics, such as PTO.[112,113] This can be considered to be an ideal system for studying the dependence of the flexoelectric effect on the piezoelectric response. Based on the isosymmetric structure and continuous octahedral rotation, we propose a model that suggests that the ferroelectric polarization gradually rotates from the monoclinically distorted T-like [0 $\underline{1}$ 1] to the R-like [$\underline{1}$11] as schematically illustrated by the blue arrows in Fig. 8(b). More interestingly, the continuous structural deformation results in a ~5× enhanced magnetism, which may result from a local flexomagnetic effect because both the R- and T-phases have a negligible canted moment. The maximum strain gradient is 5% nm^{-1} across the phase boundary; therefore, we tentatively estimate a large flexomagnetic coefficient in excess of 40 μ_B Å according to the relationship:

$$M_{flex} = \nu \frac{\partial \sigma}{\partial \chi},$$

where M_{flex} is the magnetization induced by the flexomagnetic effect and ν is the flexomagnetic coefficient. A natural conclusion is the hypothesis of a multiflexo-effect at the nanoscale phase boundaries, which includes the correlation of ferroelectric polarization, the strain gradient and the magnetic moment. In this context, a full 3-dimensional map of the strain gradient is desirable to understand the underlying physics. Several questions are apparent: how does the magnetic spin moment re-orient across the R- and T-phase boundary as described in Fig. 8(b)? Is this a means to create multiferroicity *via* a simple strain gradient and induce a flexomultiferroic effect?

In order to achieve enhanced piezoelectricity and better control of the magnetism for practical applications, it is essential to tailor the orientation, geometry and periodicity of the nanoscale phase boundaries using anisotropic stress, horizontal electric fields[114,115] or the elimination of clamping effects *via* the reduced size, *etc.* The local variation of the electronic structure may provide another tool for probing the transport[116] or photovoltaic[117] properties in the phase boundaries. Thus, these nanoscale phase boundaries have the potential to allow for the design and production of next generation, high speed, low power and high density electronic devices.

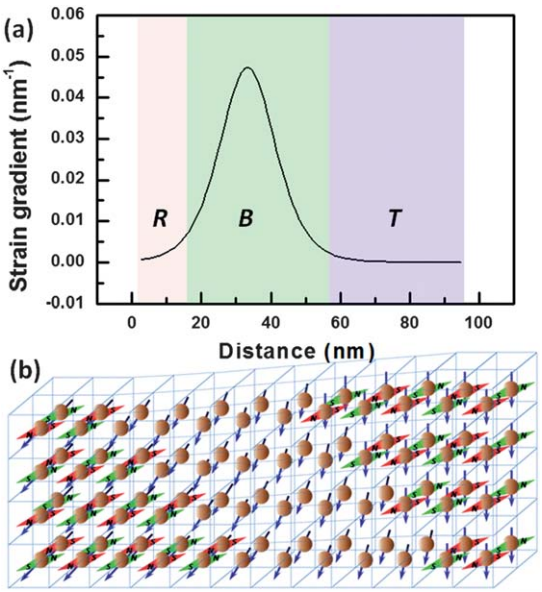

Fig. 8 (a) Strain gradient across a R-like/T-like phase boundary in a mixed-phase BFO with the R-phase as the ground state and (b) a schematic diagram of the orientation of the ferroelectric polarization and antiferromagnetic moment across the single-phase boundary.

7. Conclusions

In this article, we have summarized some recent insights on the formation of epitaxially-stabilized nanoscale phase boundaries in BFO. These mixed-phase films exhibit emergent phenomena that are absent in either parent phase, resembling a MPB as in relaxor ferroelectrics or an electronic phase separation as in the manganites and cuprates. *In situ* AFM and TEM measurements demonstrated that the phase boundaries play a critical role in the enhanced piezoelectricity. These results provide more understanding on the anomalous behaviors seen in relaxors and suggest the possibility of using mixed-phase BFO as a

replacement for lead-based piezoelectrics in micro/nanoactuators and other thin-film applications. We further demonstrated another novel property in mixed-phase BFO films in the enhanced magnetic moment at such phase boundaries. Further study revealed that this enhanced magnetic moment can be manipulated *via* an applied electric field,[68] suggesting a new route to room temperature magnetoelectric coupling in this nanoscale multiferroic system.

References

1 M. Imada, A. Fujimori and Y. Tokura, *Rev. Mod. Phys.*, 1998, **70**, 1039–1263.
2 E. Dagotto, *Rev. Mod. Phys.*, 1994, **66**, 763–840.
3 A. Moreo, S. Yunoki and E. Dagotto, *Science*, 1999, **283**, 2034–2040.
4 E. Dagotto, T. Hotta and A. Moreo, *Phys. Rep.*, 2001, **344**, 1–153.
5 G. Papavassiliou, M. Fardis, M. Belesi, T. G. Maris, G. Kallias, M. Pissas and D. Niarchos, *Phys. Rev. Lett.*, 2000, **84**, 761–764.
6 Y. Tokura, Y. Tomioka, H. Kuwahara, A. Asamitsu, Y. Moritomo and M. Kasai, *J. Appl. Phys.*, 1996, **79**, 5288–5291.
7 H. Alloul, P. Mendels, H. Casalta, J. F. Marucco and J. Arabski, *Phys. Rev. Lett.*, 1991, **67**, 3140–3143.
8 U. Welp, S. Fleshier, W. K. Kwok, R. A. Klemm, V. M. Vinokur, J. Downey, B. Veal and G. W. Crabtree, *Phys. Rev. Lett.*, 1991, **67**, 3180–3183.
9 J. H. Brewer, E. J. Ansaldo, J. F. Carolan, A. C. D. Chaklader, W. N. Hardy, D. R. Harshman, M. E. Hayden, M. Ishikawa, N. Kaplan, R. Keitel, J. Kempton, R. F. Kiefl, W. J. Kossler, S. R. Kreitzman, A. Kulpa, Y. Kuno, G. M. Luke, H. Miyatake, K. Nagamine, Y. Nakazawa, N. Nishida, K. Nishiyama, S. Ohkurna, T. M. Riseman, G. Roehmer, P. Schleger, D. Shimada, C. E. Stronach, T. Takabatake, Y. J. Uemura, Y. Watanabe, D. L. Williams, T. Yamazaki and B. Yang, *Phys. Rev. Lett.*, 1988, **60**, 1073–1076.
10 A. K. Geim, I. V. Grigorieva, S. V. Dubonos, J. G. S. Lok, J. C. Maan, A. E. Filippov and F. M. Peeters, *Nature*, 1997, **390**, 259–262.
11 S. Yang and X. Ren, *Phys. Rev. B: Condens. Matter Mater. Phys.*, 2008, **77**, 014407.
12 S. Yang, H. Bao, C. Zhou, Y. Wang, X. Ren, Y. Matsushita, Y. Katsuya, M. Tanaka, K. Kobayashi, X. Song and J. Gao, *Phys. Rev. Lett.*, 2010, **104**, 197201.
13 X. Ren and K. Otsuka, *Nature*, 1997, **389**, 579–582.
14 S. Park and T. R. Shrout, *J. Appl. Phys.*, 1997, **82**, 1804–1811.
15 E. M. Sabolsky, A. R. James, S. Kwon, S. Trolier-McKinstry and G. L. Messing, *Appl. Phys. Lett.*, 2001, **78**, 2551–2553.
16 Z. Kutnjak, J. Petzelt and R. Blinc, *Nature*, 2006, **441**, 956–969.
17 W. Liu and X. Ren, *Phys. Rev. Lett.*, 2009, **103**, 257602.
18 L. Hanh, K. Uchino, and S. Nomura, *J. Appl. Phys.*, **17**, 637–641.
19 G. Xu, J. Wen, C. Stock and P. M. Gehring, *Nat. Mater.*, 2008, **7**, 562–566.
20 J. Cao, E. Ertekin, V. Srinivasan, W. Fan, S. Huang, H. Zheng, J. W. L. Yim, D. R. Khanal, D. F. Ogletree, J. C. Grossman and J. Wu, *Nat. Nanotechnol.*, 2009, **4**, 732–737.
21 H. Gardner, A. Kumar, L. Yu, P. Xiong, M. Warusawithana, L. Wang, O. Vafek and D. Schlom, *Nat. Phys.*, 2011, **7**, 895–900.
22 P. Przyslupski, I. Komissarov, W. Paszkowicz, P. Dluzewski, R. Minikayev and M. Sawicki, *Phys. Rev. B: Condens. Matter Mater. Phys.*, 2004, **69**, 134428.
23 R. Kainuma, Y. Imano, W. Ito, Y. Sutou, H. Morito, S. Okamoto, O. Kitakami, K. Oikawa, A. Fujita, T. Kanomata and K. Ishida, *Nature*, 2006, **439**, 957–960.
24 J. F. Tressler, S. Alkoy and R. Newnham, *J. Electroceram.*, 1998, **2**, 257–272.
25 Y.-M. Chiang, G. Farrey and A. Soukhojak, *Appl. Phys. Lett.*, 1998, **73**, 3683–3685.
26 H. Fu and R. Cohen, *Nature*, 2000, **403**, 281–283.
27 Y. Saito, H. Takao, T. Tani, T. Nonoyama, K. Takatori, T. Homma, T. Nagaya and M. Nakamura, *Nature*, 2004, **432**, 84–87.
28 Z. Wu and R. Cohen, *Phys. Rev. Lett.*, 2005, **95**, 037601.
29 M. Ahart, M. Somayazulu, R. Cohen, P. Ganesh, P. Dera, H. K. Mao, R. J. Hemley, Y. Ren, P. Liermann and Z. Wu, *Nature*, 2008, **451**, 545–U2.
30 J. Wang, J. B. Neaton, H. Zheng, V. Nagarajan, S. B. Ogale, B. Liu, D. Viehland, V. Vaithyanathan, D. Schlom, U. Waghmare, N. A. Spaldin, K. M. Rabe, M. Wuttig and R. Ramesh, *Science*, 2003, **299**, 1719–1722.
31 H. N. Lee, H. M. Christen, M. F. Chisholm, C. M. Rouleau and D. H. Lowndes, *Nature*, 2005, **433**, 395–399.
32 J. H. Haeni, P. Irvin, W. Chang, R. Uecker, P. Reiche, Y. L. Li, S. Choudhury, W. Tian, M. E. Hawley, B. Craigo, A. K. Tagantsev, X. Q. Pan, S. K. Streiffer, L. Q. Chen, S. W. Kirchoefer, J. Levy and D. G. Schlom, *Nature*, 2004, **430**, 758–761.
33 A. R. Chaudhuri, M. Arredondo, A. Hahne, A. Morelli, M. Becker, M. Alexe and I. Vrejoiu, *Phys. Rev. B: Condens. Matter Mater. Phys.*, 2011, **84**, 054112.
34 C. Thiele, K. Dörr, O. Bilani, J. Rödel and L. Schultz, *Phys. Rev. B: Condens. Matter Mater. Phys.*, 2007, **75**, 054408.
35 I. Bozovic, G. Logvenov, I. Belca, B. Narimbetov and I. Sveklo, *Phys. Rev. Lett.*, 2002, **89**, 107001.
36 C. W. Bark, D. A. Felker, Y. Wang, Y. Zhang, H. W. Jang, C. M. Folkman, J. W. Park, S. H. Baek, H. Zhou, D. D. Fong, X. Q. Pan, E. Y. Tsymbal, M. S. Rzchowski and C. B. Eom, *Proc. Natl. Acad. Sci. U. S. A.*, 2011, **108**, 4720.
37 T. Zhao, A. Scholl, F. Zavaliche, K. Lee, M. Barry, A. Doran, M. P. Cruz, Y. H. Chu, C. Ederer, N. A. Spaldin, R. R. Das, D. M. Kim, S. H. Baek, C. B. Eom and R. Ramesh, *Nat. Mater.*, 2006, **5**, 823–829.
38 Y. H. Chu, L. W. Martin, M. B. Holcomb, M. Gajek, S. J. Han, Q. He, N. Balke, C. H. Yang, D. Lee, W. Hu, Q. Zhan, P. L. Yang, A. Fraile-Rodriguez, A. Scholl, S. X. Wang and R. Ramesh, *Nat. Mater.*, 2008, **7**, 478–482.
39 C. Ederer and N. A. Spaldin, *Phys. Rev. Lett.*, 2005, **95**, 257601.
40 D. Ricinschi, K.-Y. Yun and M. Okuyama, *J. Phys.: Condens. Matter*, 2006, **18**, L97–L105.
41 P. Ravindran, R. Vidya, O. Eriksson and H. Fjellvag, *Adv. Mater.*, 2008, **20**, 1353–1356.
42 R. V. Shpanchenko, V. V. Chernaya, A. A. Tsirlin, P. S. Chizhov, D. E. Sklovsky, E. V. Antipov, E. P. Khlybov, V. Pomjakushin, A. M. Balagurov, J. E. Medvedeva, E. E. Kaul and C. Geibel, *Chem. Mater.*, 2004, **16**, 3267–3273.
43 J. Kreisel, P. Jadhav, O. Chaix-Pluchery, M. Varela, N. Dix, F. Sanchez and J. Fontcuberta, *J. Phys.: Condens. Matter*, 2011, **23**, 342202.
44 H. M. Christen, J. H. Nam, H. S. Kim, A. J. Hatt and N. A. Spaldin, *Phys. Rev. B: Condens. Matter Mater. Phys.*, 2011, **83**, 144107.
45 Z. Chen, Z. Luo, Y. Qi, P. Yang, S. Wu, C. Huang, T. Wu, J. Wang, C. Gao, T. Sritharan and L. Chen, *Appl. Phys. Lett.*, 2010, **97**, 242903.
46 M. N. Iliev, M. V. Abrashev, D. Mazumdar, V. Shelke and A. Gupta, *Phys. Rev. B: Condens. Matter Mater. Phys.*, 2010, **82**, 014107.
47 C.-J. Cheng, C. Lu, Z. Chen, L. You, L. Chen, J. Wang and T. Wu, *Appl. Phys. Lett.*, 2011, **98**, 242502.
48 Z. Chen, Z. Luo, C. Huang, Y. Qi, P. Yang, L. You, C. Hu, T. Wu, J. Wang, C. Gao, T. Sritharan and L. Chen, *Adv. Funct. Mater.*, 2011, **21**, 133–138.
49 D. Mazumdar, V. Shelke, M. Iliev, S. Jesse, A. Kumar, S. V. Kalinin, A. P. Baddorf and A. Gupta, *Nano Lett.*, 2010, **10**, 2555–2561.
50 R. K. Vasudevan, Y. Liu, J. Li, W.-I. Liang, A. Kumar, S. Jesse, Y.-C. Chen, Y.-H. Chu, V. Nagarajan and S. V. Kalinin, *Nano Lett.*, 2011, **11**, 3346–3354.
51 H. Y. Kuo, Y. C. Shu, H. Z. Chen, C. J. Hsueh, C. H. Wang and Y. H. Chu, *Appl. Phys. Lett.*, 2010, **97**, 242906.
52 Z. Chen, S. Prosandeev, Z. L. Luo, W. Ren, Y. Qi, C. W. Huang, L. You, C. Gao, I. A. Kornev, T. Wu, J. Wang, P. Yang, T. Sritharan, L. Bellaiche and L. Chen, *Phys. Rev. B: Condens. Matter Mater. Phys.*, 2011, **84**, 094116.
53 C. W. Huang, Y. H. Chu, Z. H. Chen, J. Wang, T. Sritharan, Q. He, R. Ramesh and L. Chen, *Appl. Phys. Lett.*, 2010, **97**, 152901.
54 A. L. Roytburd, J. Ouyang, B. M. Boyerinas and H. A. Bruck, *Appl. Phys. Lett.*, 2011, **99**, 172902.
55 P. Chen, N. J. Podraza, X. S. Xu, A. Melville, E. Vlahos, V. Gopalan, R. Ramesh, D. G. Schlom and J. L. Musfeldt, *Appl. Phys. Lett.*, 2010, **96**, 131907.

56 A. Kumar, S. Denev, R. J. Zeches, E. Vlahos, N. J. Podraza, A. Melville, D. G. Schlom, R. Ramesh and V. Gopalan, *Appl. Phys. Lett.*, 2010, **97**, 112903.
57 R. J. Zeches, M. D. Rossell, J. X. Zhang, A. J. Hatt, Q. He, C.-H. Yang, A. Kumar, C. H. Wang, A. Melville, C. Adamo, G. Sheng, Y.-H. Chu, J. F. Ihlefeld, R. Erni, C. Ederer, V. Gopalan, L. Q. Chen, D. G. Schlom, N. A. Spaldin, L. W. Martin and R. Ramesh, *Science*, 2009, **326**, 977–980.
58 J. Ouyang, W. Zhang, X. Huang and A. L. Roytburd, *Acta Mater.*, 2011, **59**, 3779–3791.
59 D. G. Schlom, L.-Q. Chen, X. Pan, A. Schmehl and M. A. Zurbuchen, *J. Am. Ceram. Soc.*, 2008, **91**(8), 2429–2454.
60 M. D. Biegalski, J. H. Haeni, S. Trolier-McKinstry, D. G. Schlom, C. D. Brandle and A. J. Ven Graitis, *J. Mater. Res.*, 2005, **20**, 952–958.
61 I. C. Infante, S. Lisenkov, B. Dupe, M. Bibes, S. Fusil, E. Jacquet, G. Geneste, S. Petit, A. Courtial, J. Juraszek, L. Bellaiche, A. Barthelemy and B. Dkhil, *Phys. Rev. Lett.*, 2010, **105**, 057601.
62 H. Bea, B. Dupe, S. Fusil, R. Mattana, E. Jacquet, B. Warot-Fonrose, F. Wilhelm, A. Rogalev, S. Petit, V. Cros, A. Anane, F. Petroff, K. Bouzehouane, G. Geneste, B. Dkhil, S. Lisenkov, I. Ponomareva, L. Bellaiche, M. Bibes and A. Barthelemy, *Phys. Rev. Lett.*, 2009, **102**, 217603.
63 H. W. Jang, S. H. Baek, D. Ortiz, C. M. Folkman, R. R. Das, Y. H. Chu, P. Shafer, J. X. Zhang, S. Choudhury, V. Vaithyanathan, Y. B. Chen, D. A. Felker, M. D. Biegalski, M. S. Rzchowski, X. Q. Pan, D. G. Schlom, L. Q. Chen, R. Ramesh and C. B. Eom, *Phys. Rev. Lett.*, 2008, **101**, 107602.
64 D. S. Rana, K. Takahashi, K. R. Mavani, I. Kawayama, H. Murakami, M. Tonouchi, T. Yanagida, H. Tanaka and T. Kawai, *Phys. Rev. B: Condens. Matter Mater. Phys.*, 2007, **75**, 060405(R).
65 C. Ederer and N. A. Spaldin, *Phys. Rev. B: Condens. Matter Mater. Phys.*, 2005, **71**, 060401.
66 P. Fisher, M. Polomska, I. Sosnowska and M. Szymański, *J. Phys. C: Solid State Phys.*, 1980, **13**, 1931.
67 J. X. Zhang, Q. He, M. Trassin, W. Luo, D. Yi, M. D. Rossell, P. Yu, L. You, C. H. Wang, C. Y. Kuo, J. T. Heron, Z. Hu, R. J. Zeches, H. J. Lin, A. Tanaka, C. T. Chen, L. H. Tjeng, S. Salahuddin, Y.-H. Chu and R. Ramesh, *Phys. Rev. Lett.*, 2011, **107**, 147602; B. Dupé, I. C. Infante, G. Geneste, P.-E. Janolin, M. Bibes, A. Barthélémy, S. Lisenkov, L. Bellaiche, S. Ravy and B. Dkhil, *Phys. Rev. B: Condens. Matter Mater. Phys.*, 2010, **81**, 144128.
68 Q. He, Y. H. Chu, J. T. Heron, S. Y. Yang, W. I. Liang, C. Y. Kuo, H. J. Lin, P. Yu, C. W. Liang, R. J. Zeches, W. C. Kuo, J. Y. Juang, C. T. Chen, E. Arenholz, A. Scholl and R. Ramesh, *Nat. Commun.*, 2011, **2**, 225.
69 J. F. Scott, *Adv. Mater.*, 2010, **22**, 2106–2107.
70 J. F. Scott, *J. Phys.: Condens. Matter*, 2011, **23**, 022202.
71 A. J. Hatt, N. A. Spaldin and C. Ederer, *Phys. Rev. B: Condens. Matter Mater. Phys.*, 2010, **81**, 054109.
72 A. G. Christy, *Acta Crystallogr., Sect. B: Struct. Sci.*, 1995, **51**, 753–757.
73 S. Lisenkov, D. Rahmedov and L. Bellaiche, *Phys. Rev. Lett.*, 2009, **103**, 0487204.
74 J. F. Scott, *Rev. Mod. Phys.*, 1974, **46**, 83.
75 R. A. Cowley, *Phys. Rev. B: Solid State*, 1976, **13**, 4877.
76 I. L. Aptekar, V. I. Rashupkin and E. Y. Tonkov, *Fizika Tverdogo Tela*, 1979, **21**, 1556.
77 A. Jayaraman, *Phys. Rev.*, 1965, **137**, A179.
78 A. Jayaraman, D. B. McWhan, J. P. Remeika and P. D. Dernier, *Physical Review A: Atomic, Molecular, and Optical Physics*, 1970, **B2**, 3751.
79 Y. Ishibashi and Y. Hidaka, *J. Phys. Soc. Jpn.*, 1991, **60**, 1634.
80 Y. Ishibashi and M. Iwata, *J. Phys. Soc. Jpn.*, 2002, **71**, 2576.
81 J. M. Rondinelli and S. Coh, *Phys. Rev. Lett.*, 2011, **106**, 235502; W. Siemons, M. D. Biegalski, J. H. Nam and H. M. Christen, *Appl. Phys. Express*, 2011, **4**, 095801; A. R. Damodaran, S. Lee, J. Karthik, S. MacLaren and L. W. Martin, *Phys. Rev. B: Condens. Matter Mater. Phys.*, 2012, **85**, 024113; A. R. Damodaran, E. Breckenfeld, A. K. Choquette and L. W. Martin, *Appl. Phys. Lett.*, 2012, **100**, 082904; J. Kreisel, P. Jadhav, O. Chaix-Pluchery, M. Varela, N. Dix, F. Sanchez and J. Fontcuberta, *J. Phys.: Condens. Matter*, 2011, **23**, 342202.
82 Y. Y. Liu and J. Y. Li, *Phys. Rev. B: Condens. Matter Mater. Phys.*, 2011, **84**, 132104.
83 G. H. Haertling, *J. Am. Ceram. Soc.*, 1999, **82**(4), 797–818.
84 Y. Xu, *Ferroelectric Materials and Their Applications*, Elsevier Science Publishers, Amsterdam, 1991.
85 R. Bechmann, *Phys. Rev.*, 1958, **110**, 1060–1061.
86 S. Roberts, *Phys. Rev.*, 1947, **71**, 890–895.
87 X.-H. Du, J. Zheng, U. Belegundu and K. Uchino, *Appl. Phys. Lett.*, 1998, **72**, 2421–2423.
88 T. Takenaka and H. Nagata, *J. Eur. Ceram. Soc.*, 2005, **25**, 2693–2700.
89 B. Noheda, *Curr. Opin. Solid State Mater. Sci.*, 2002, **6**, 9.
90 J. Frantti, *J. Phys. Chem. B*, 2008, **112**, 6521.
91 B. Noheda, D. E. Cox, G. Shirane, J. Gaoand and Z.-G. Ye, *Phys. Rev. B: Condens. Matter*, 2002, **66**, 054104.
92 X. Ren, *Nat. Mater.*, 2004, **3**, 91–94.
93 J. X. Zhang, B. Xiang, Q. He, J. Seidel, R. J. Zeches, P. Yu, S. Y. Yang, C. H. Wang, Y.-H. Chu, L. W. Martin, A. M. Minor and R. Ramesh, *Nat. Nanotechnol.*, 2011, **6**, 98–102.
94 X. Tan and J. S. Baras, *Automatica*, 2004, **40**, 1469–1480.
95 V. Nagarajan, A. Roytburd, A. Stanishevsky, S. Prasertchoung, T. Zhao, L. Chen, J. Melngailis, O. Auciello and R. Ramesh, *Nat. Mater.*, 2002, **2**, 43–47.
96 M. Chmielus, X. X. Zhang, C. Witherspoon, D. C. Dunand and P. Müllner, *Nat. Mater.*, 2009, **8**, 863–866.
97 Z. Ma, F. Zavaliche, L. Chen, J. Ouyang, J. Melngailis, A. L. Roytburd, V. Vaithyanathan, D. G. Schlom, T. Zhao and R. Ramesh, *Appl. Phys. Lett.*, 2005, **87**, 072907.
98 T. Kimura, T. Goto, H. Shintani, K. Ishizaka, T. Arima and Y. Tokura, *Nature*, 2003, **426**, 55–58.
99 M. Fiebig, *J. Phys. D: Appl. Phys.*, 2005, **38**, R123–R152.
100 S. W. Cheong and M. Mostovoy, *Nat. Mater.*, 2007, **6**, 13–20.
101 R. Ramesh and N. A. Spaldin, *Nat. Mater.*, 2007, **6**, 21–29.
102 S. M. Wu, S. A. Cybart, P. Yu, M. D. Rossell, J. X. Zhang, R. Ramesh and R. C. Dynes, *Nat. Mater.*, 2010, **9**, 756–761.
103 P. Yu, J.-S. Lee, S. Okamoto, M. D. Rossell, M. Huijben, C.-H. Yang, Q. He, J. X. Zhang, S. Y. Yang, M. J. Lee, Q. M. Ramasse, R. Erni, Y.-H. Chu, D. A. Arena, C.-C. Kao, L. W. Martin and R. Ramesh, *Phys. Rev. Lett.*, 2010, **105**, 027201.
104 J. T. Heron, M. Trassin, K. Ashraf, M. Gajek, Q. He, S. Y. Yang, D. E.Nikonov, Y. H. Chu, S. Salahuddin and R. Ramesh, *Phys. Rev. Lett.*, 2011, **107**, 217202.
105 N. A. Hill, *J. Phys. Chem. B*, 2000, **104**, 6694–6709.
106 Y. E. Roginska, Y. Y. Tomashpo, Y. N. Venevtse, V. M. Petrov and G. S. Zhdanov, *Soviet Physics - JETP*, 1966, **23**, 47–51.
107 S. V. Kiselev, R. P. Ozerov and G. S. Zhdanov, *Sov. Phys. Dokl*, 1963, **7**, 742–744.
108 I. Sosnowska, M. Loewenhaupt, W. I. E. David and R. M. Ibberson, *Phys. B*, 1992, **180**, 117–118; G. J. MacDougall, H. M. Christen, W. Siemons, M. D. Biegalski, J. L. Zarestky, S. Liang, E. Dagotto and S. E. Nagler, *Phys. Rev. B: Condens. Matter Mater. Phys.*, 2012, **85**, 100406(R).
109 F. de Groot, *Chem. Rev.*, 2001, **101**, 1779–1808.
110 M. Ramazanoglu, W. Ratcliff, Y. J. Choi, S. Lee, S. W. Cheong and V. Kiryukhin, *Phys. Rev. B: Condens. Matter Mater. Phys.*, 2011, **83**, 174434.
111 Y. X. Lu, J. S. Claydon, Y. B. Xu, S. M. Thompson, K. Wilson and G. van der Laan, *Phys. Rev. B: Condens. Matter Mater. Phys.*, 2004, **70**, 2333–2334.
112 G. Catalan, A. Lubk, A. H. G. Vlooswijk, E. Snoeck, C. Magen, A. Janssens, G. Rispens, G. Rijnders, D. H. A. Blank and B. Noheda, *Nat. Mater.*, 2011, **10**, 963–967.
113 D. Lee, A. Yoon, S. Y. Jang, J. G. Yoon, J. S. Chung, M. Kim, J. F. Scott and T. W. Noh, *Phys. Rev. Lett.*, 2011, **107**, 057602.
114 Y.-C. Chen, Q. He, F.-N. Chu, Y.-C. Huang, J.-W. Chen, W.-I. Liang, R. K. Vasudevan, V. Nagarajan, E. Arenholz, S. V. Kalinin and Y.-H. Chu, *Adv. Mater.*, 2012, **24**, 3070.
115 A. R. Damodaran, C.-W. Liang, Q. He, C.-Y. Peng, L. Chang, Y.-H. Chu and L. W. Martin, *Adv. Mater.*, 2011, **23**, 3170.
116 J. Seidel, L. W. Martin, Q. He, Q. Zhan, Y.-H. Chu, A. Rother, M. E. Hawkridge, P. Maksymovych, P. Yu, M. Gajek, N. Balke, S. V. Kalinin, S. Gemming, F. Wang, G. Catalan, J. F. Scott, N. A. Spaldin, J. Orenstein and R. Ramesh, *Nat. Mater.*, 2009, **8**, 229–234.
117 S. Y. Yang, J. Seidel, S. J. Byrnes, P. Shafer, C.-H. Yang, M. D. Rossell, P. Yu, Y.-H. Chu, J. F. Scott, J. W. Ager, L. W. Martin and R. Ramesh, *Nat. Nanotechnol.*, 2010, **5**, 143–147.

